Star Formation News Letter:No.303 #29-38

2018.05.18 寺澤祥子

29. Unlocking CO Depletion in Protoplanetary Disks I. The Warm Molecular Layer
30. A Statistical Study of Massive Cluster-Forming Clumps
31. Sun-Sized Water Vapor Masers in Cepheus A
32. Subsonic islands within a high-mass star-forming IRDC
33. Triggering the formation of the supergiant HII region NGC 604 in M33
34. Helical Magnetic Fields in Molecular Clouds? A New Method to Determine the Line-of-Sight Magnetic Field Structure in Molecular Clouds
35. The Envelope Kinematics and a Possible Disk Around the Class 0 Protostar within BHR7
36. Dancing twins: stellar hierarchies that formed sequentially?
37. The Massive Star-Forming Regions Omnibus X-Ray Catalog, Second Installment
38. Inward Migration of the TRAPPIST-1 Planets as Inferred From Their Water-Rich Compositions

#32　Subsonic islands within a high-mass star-forming IRDC

Vlas Sokolov, KeWang, Jaime E. Pineda, Paola Caselli, Jonathan D. Henshaw, Ashley T. Barnes, Jonathan C. Tan, Francesco Fontani, Izaskun Jim´enez-Serra and Qizhou Zhang

導入・目的

- 大質量星の星形成領域は超音速運動に支配される
  星形成領域内の密度が高いコアに向かって、乱流が散逸して星形成が生じる
- 大質量星の星形成には、非熱的なガス運動(散逸手前の状態)を伴う
  非熱運動は、大質量星形成の乱流コアモデルにおいて重要要素
  乱流運動が重力崩壊をもたらし、ガスの降着速度をより速めるため
- 低質量星と比較すると、高質量星のデータは少ない

観測天体

- G035.39-00-33 (G035.39 henceforth)：IRDC(Infrared dark cloud)
  COの非熱運動速度が音速の中央値よりも２～３倍速い
  地球との距離：2.9kpc、天体の大きさ：6.8pc (Simon et al. 2006)
- CASAのタスクのTCLEANよりデコンボリューション
- VLAの単一鏡のデータで足りないフラックスデータをGBTで補正

Telescope	VLA(Very Large Telescope)+GBT(Green Bank Telescope)
Date	2010年5月8日
EmissionLine	$NH_3(1,1)\&(2,2)$(23GHz)
Resolution	15.625kHz

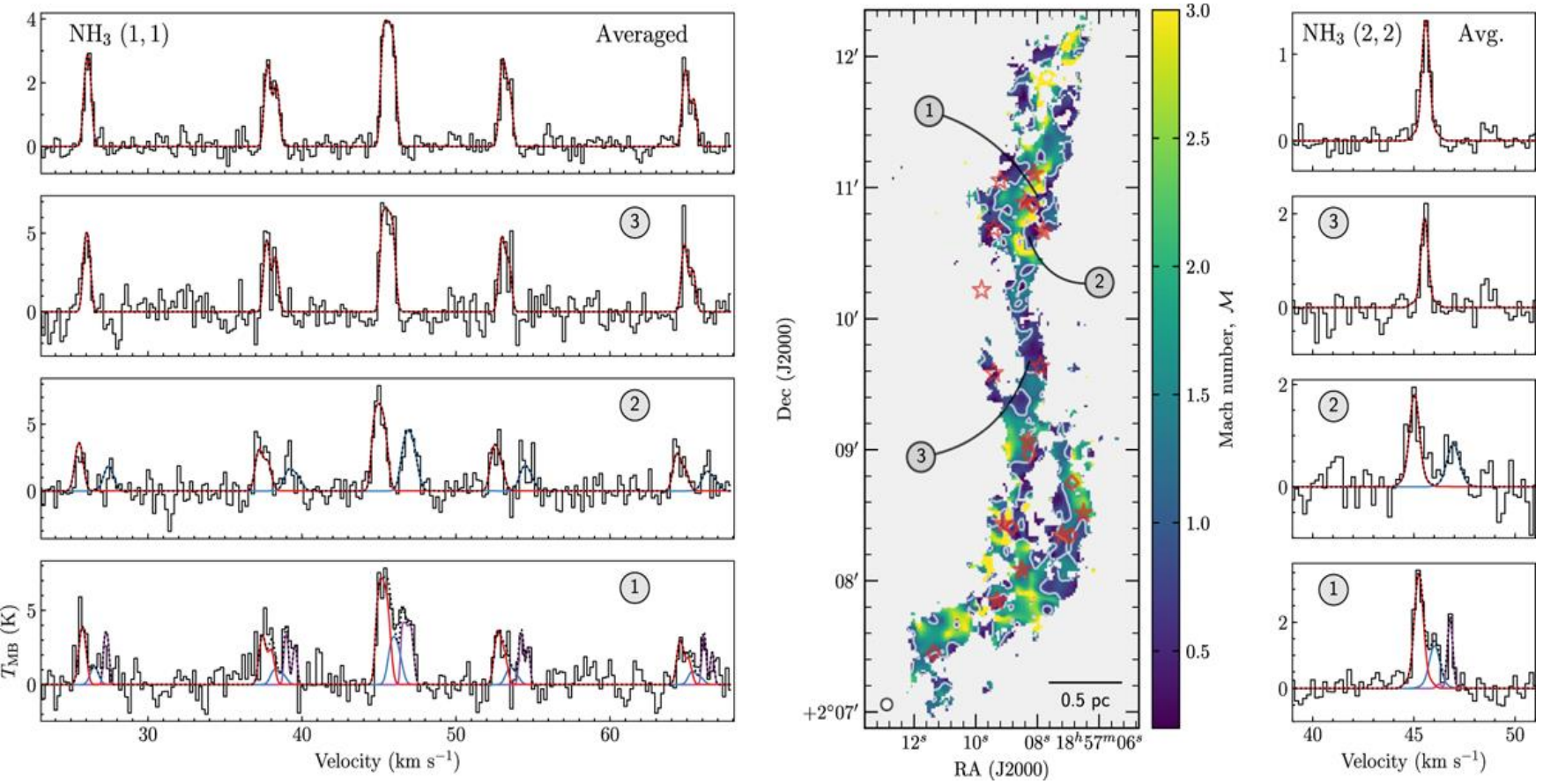

（中央）マッハ数の空間分図
（左右）$NH_3(1,1)$&$(2,2)$スペクトル

結果

マッハ数の空間分布
・M<1(非熱ガス運動)：38.8%

・1<M<2（超音速）：42%

・M>2：9.2%

(平均温度12K,標準偏差2.2Kで
フィッテイングされた温度を利用)

考察

- 全NH_3成分のマッハ数の分布と規格化された密度をプロット。
  結果、マッハ数のピークはM=0.91、
  星形成開始前段階の「starlessコア」のNH_3線幅は0.35km/s
  (IRDCの「starlessコア」のNH_3線幅は平均1.0km/s)

- 今回のデータのNH_3線幅より得られること
  IRDC内の乱流が減少し、重力崩壊が起きている可能性
  - G035.39の亜音速領域内がビリアル平衡状態であるには、1.5~2mGの莫大な磁場強度が必要（Tan et al（2013））
  - だが、初期段階のIRDCとG035.39の磁場強度が似たorderであり、莫大なものではなかった
  - 今回のTargetでは幾つかの原始星源があるので、IRDCの一部は既に不安定or重力崩壊中と考えられる

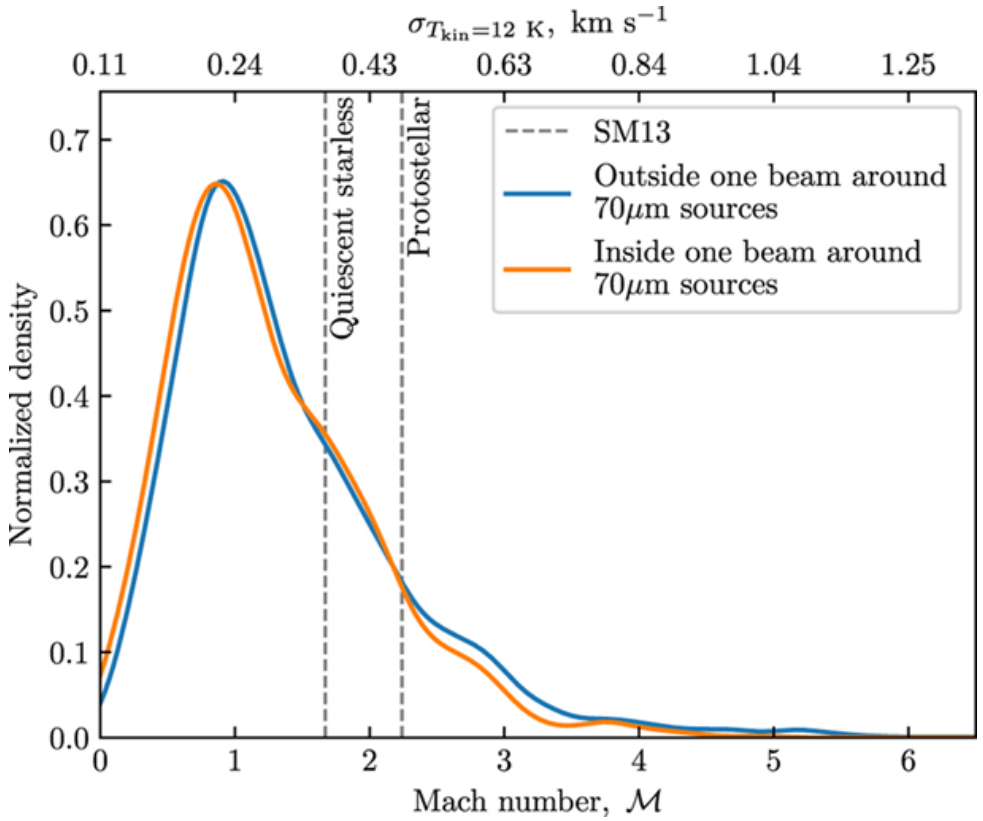

G035.39の非熱運動線幅と音速比率のカーネル密度図

#35 The Envelope Kinematics and a Possible Disk Around the Class 0 Protostar within BHR7

John J. Tobin, Steven P. Bos, Michael M. Dunham, Tyler L. Bourke, Nienke van der Marel

導入・目的

- 原始星の質量は外層のガスの降着によって増え、星の成長を更に促す。円盤が大きければ、重力不安定性で断片化される
- 原始惑星系円盤の形成と進化を知るためには星形成を通じて観測する必要がある
- しかし、原始星を取り巻くエンベロープと原始惑星系円盤の区別をするのは難しい

観測天体

- BHR7：Dark Cloud
  原始星が1つしかない独立した分子雲
  原始星同士の相互相関の影響がほぼ無い
- 地球との距離：400~500pc（Woermann et al.2001）
- 計5種類の望遠鏡のデータを使用
  中でもSMAのデータをメインに使用する

Telescope	Date	EmissionLine,Wavelength
SMA (Submillimeter Array)	2015 ~ 2016年に数度	1.3mm連続波 ^{12}CO, ^{13}CO, $C^{18}O$, H_2CO, N_2D^+,SO,SiO
Herschel Space Observatory	2010年	下表
Spitzer Space Telescope	2008年12月22日	3.6,4.5,5.8および8.0μm
CTIO (Cerro-Tololo Inter-American Observatory)	2009年6月11日	J（1.25μm）、H（1.6μm）、Ks（2.15μm）バンド
SEST (Swedish-ESO Submillimetre Telescope)	2001年6月～2003年8月	1.2mm（250GHz）連続波

Table 1
SMA Observations

Source	R.A. (J2000)	Decl. (J2000)	Config.[a]	Date (UT)	Calibrators (Gain, Flux)
BHR7	8:14:23.326	−34:31:05.7	VEX	2015 Jan 28	0747-311, Callisto
BHR7	8:14:23.33	−34:31:03.7	COMP	2015 Dec 25	0747-331, Uranus
BHR7	8:14:23.33	−34:31:03.7	EXT	2016 Apr 02	0747-311, Ganymede

Note. The position listed for VEX corresponds to the phase center of the observations, not the coordinates of the continuum emission, and the positions for EXT and COMP are centered on the continuum source.
[a] VEX—Very Extended, EXT—Extended, and COMP—Compact.

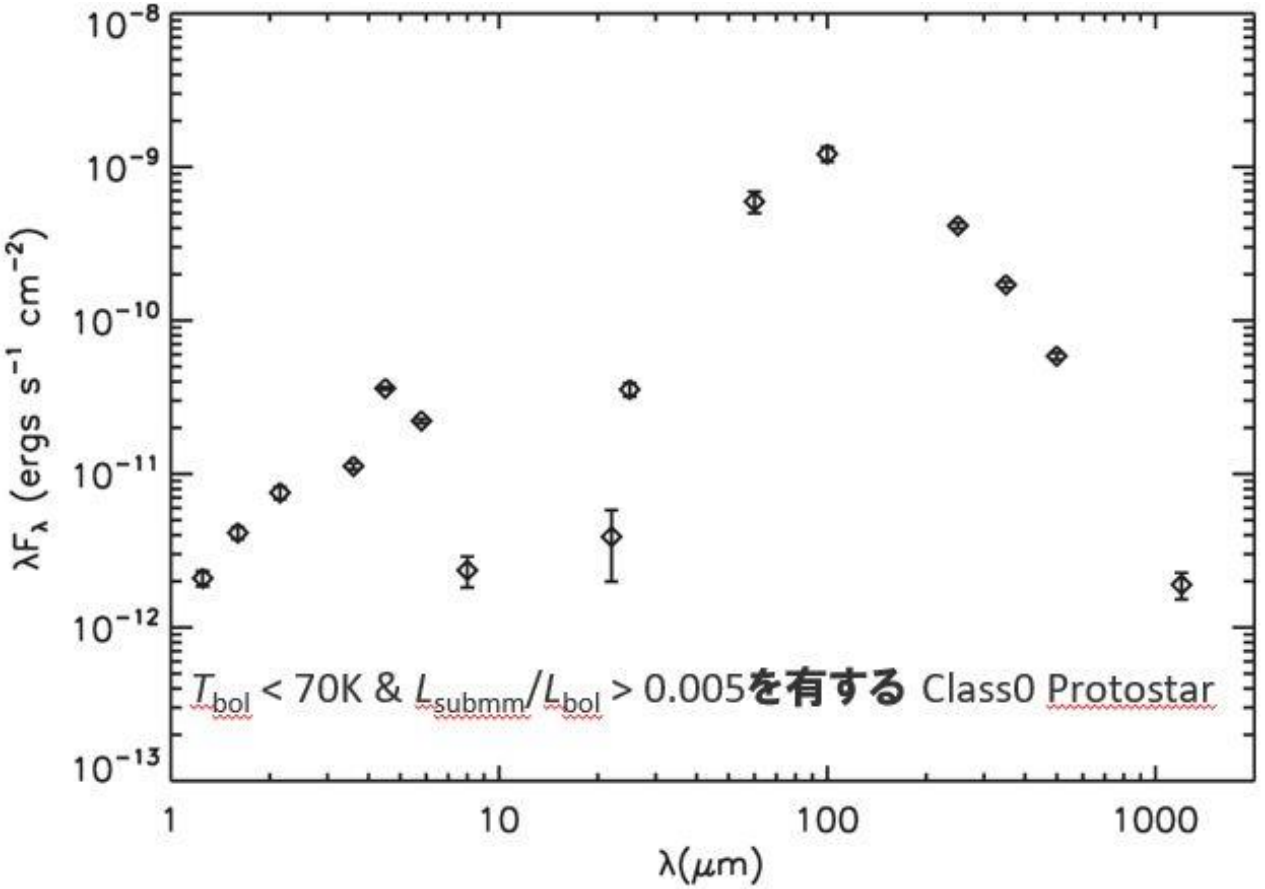

BHR7のスペクトルエネルギー分布図

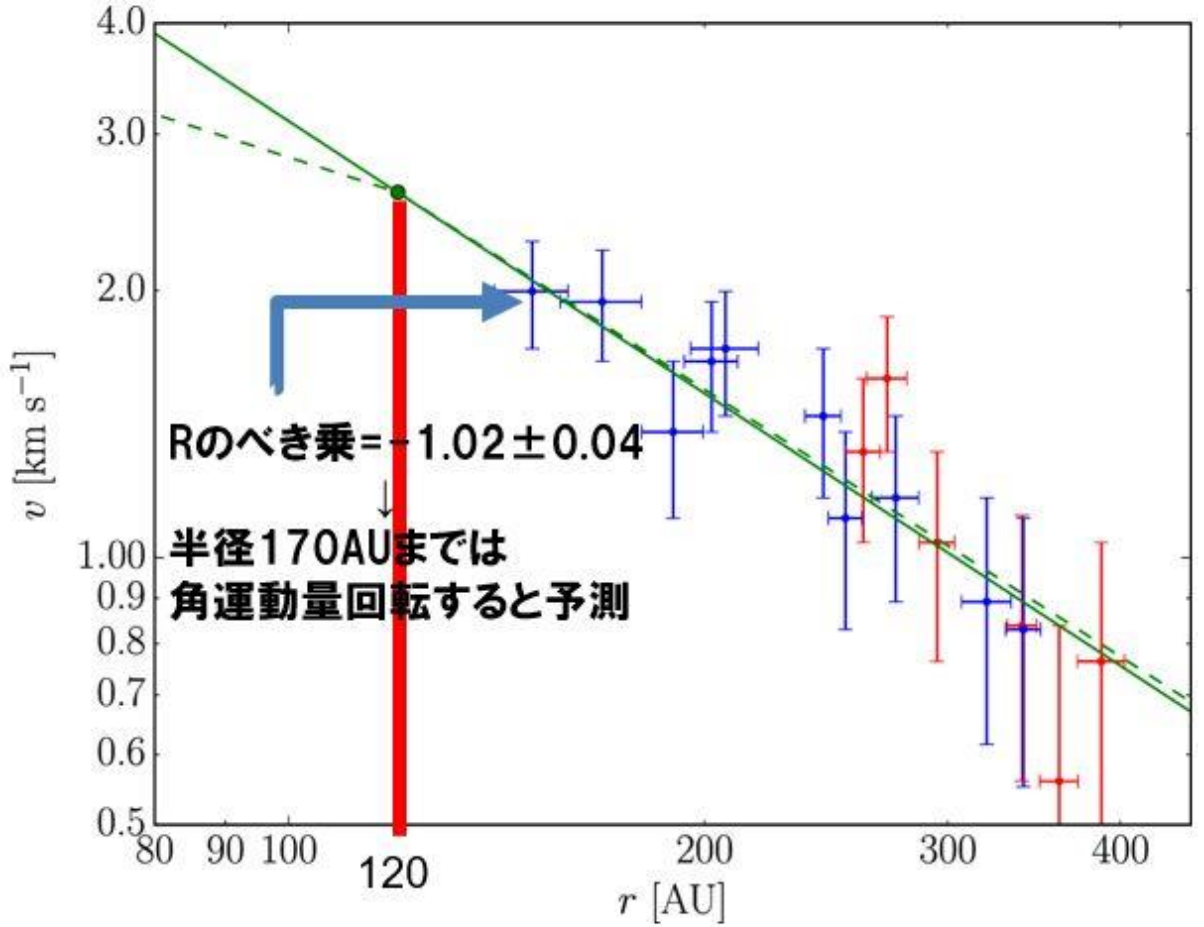

BHR7のピークPV図（緑線は回転運動直線）

結果

1. SEDより、
   - ボロメトリック光度：9.3 $L_\odot$
   - ボロメトリック温度：50.5K
   - 全輻射光度比率：0.034

   ↓

   Class0の原始星の基準を満たす

2. BHR7のピークPV図より、
   - 回転運動曲線のRのべき乗が約-1に比例
     角運動量回転を行う可能性が高い
   - 120AUより内側の領域でケプラー回転が発見される

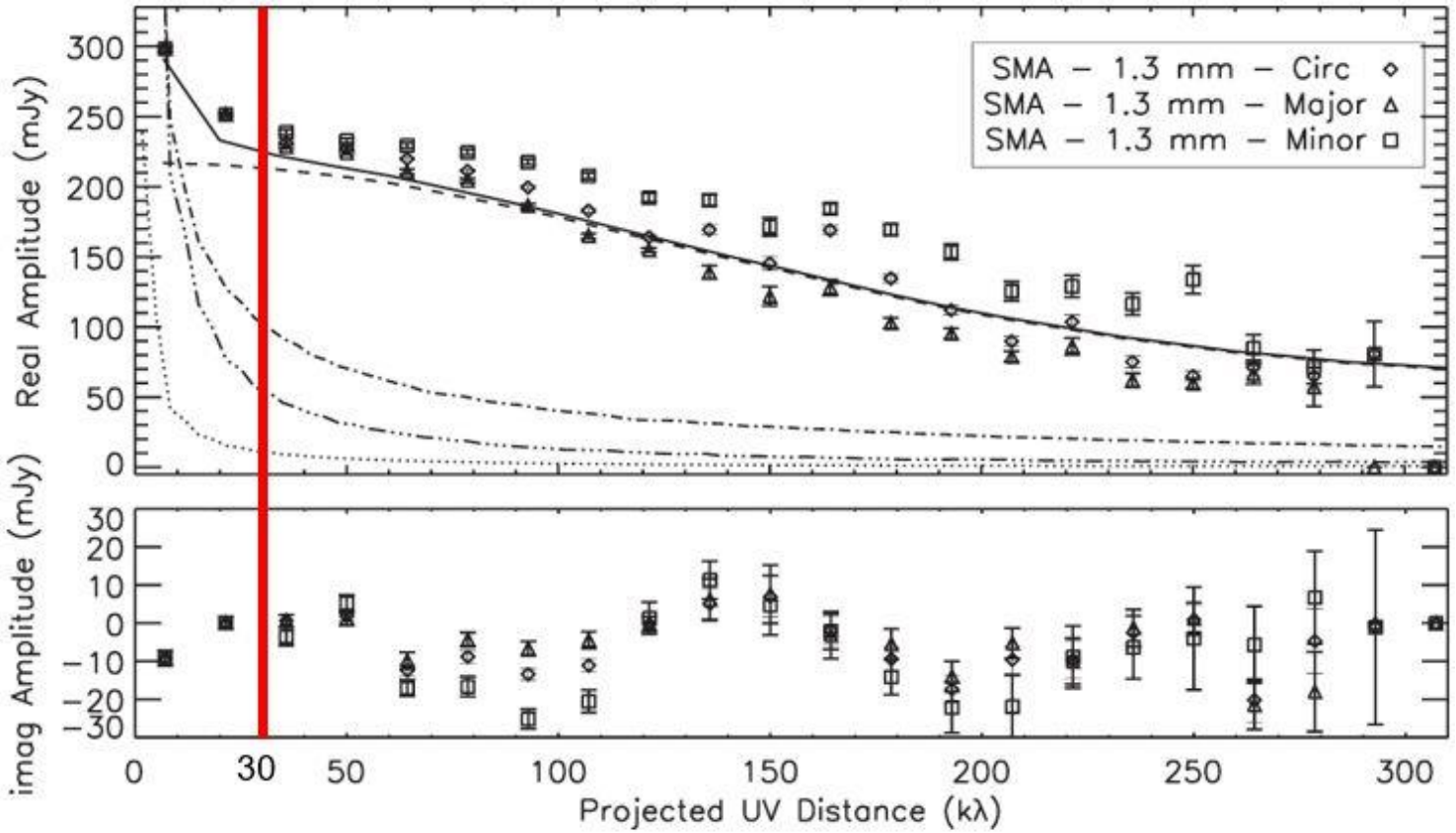

SMAデータセットでのuv平面内の円形平均視界振幅とカットの両方を示す図

3. ビジビリティの振幅概形

3回のSMA観測のビジビリティデータをそれぞれ実数領域と虚数領域にわけ、振幅とUV平面距離の図として示す

- 実数領域でのUV平面距離>50kλ
  いずれのデータも発散を始める
- 実数領域でのUV平面距離>200kλ
  いずれのデータも平坦な構造をとる
- 虚数領域
  100kλ起きの周期がみられる

以上の要点を満たすように円盤のモデルを形成したところ、

$R_{disk} = 100\mathrm{AU}$　$M_{disk} = 0.47M_{\odot}$

となった

考察

1. BHR7の原始星の質量

原始惑星系円盤がケプラー運動を行っている場合、この半径を仮定することで原子星の質量を推定可能。
今回はPV図より、ケプラー半径が120AU、回転速度は2.58km/sと仮定
$v = (GM/R)^{0.5}$に代入すると、原始星は約「$1M_{\odot}$」であると判明した

2. 重力不安定性について

回転系の安定性の解析には、Toomre'sのQ値と呼ばれる式を用いる。

$$Q \approx 2\frac{M_*}{M_d}\frac{H}{r}.$$

（Hは円盤系の高さ）

この式のQの値が1よりも大きい場合、重力崩壊に対して安定性を持つ。
BHR 7 の場合、Q≒0.4であることから、重力不安定性である可能性がある
だが、今回用いているBHR7と地球との距離は不確実性である
その為、円盤や原始星の質量が大きく変化する可能性も高く、Qの値が変化する可能性もまたある

#36 Dancing twins: stellar hierarchies that formed sequentially?

Andrei Tokovinin

概要

- Double-twin形成のシナリオは大きく2つある
  1. 内側から外側へと形成される場合（図の左）
     伴星Aは内側の連星の総質量と同等の大きさまで成長できる
  2. 階層的に構築される場合（図の右）
     回転している分子雲が、等分に断片化されることで連星が形成する

- 多階層においての質量と軌道の特徴づけは、どちらの形成シナリオなのかを決定するのに重要。
  今回は、低質量星からなる4つの独立した階層系で観測された内側と外側のケプラー運動によってモデル化する

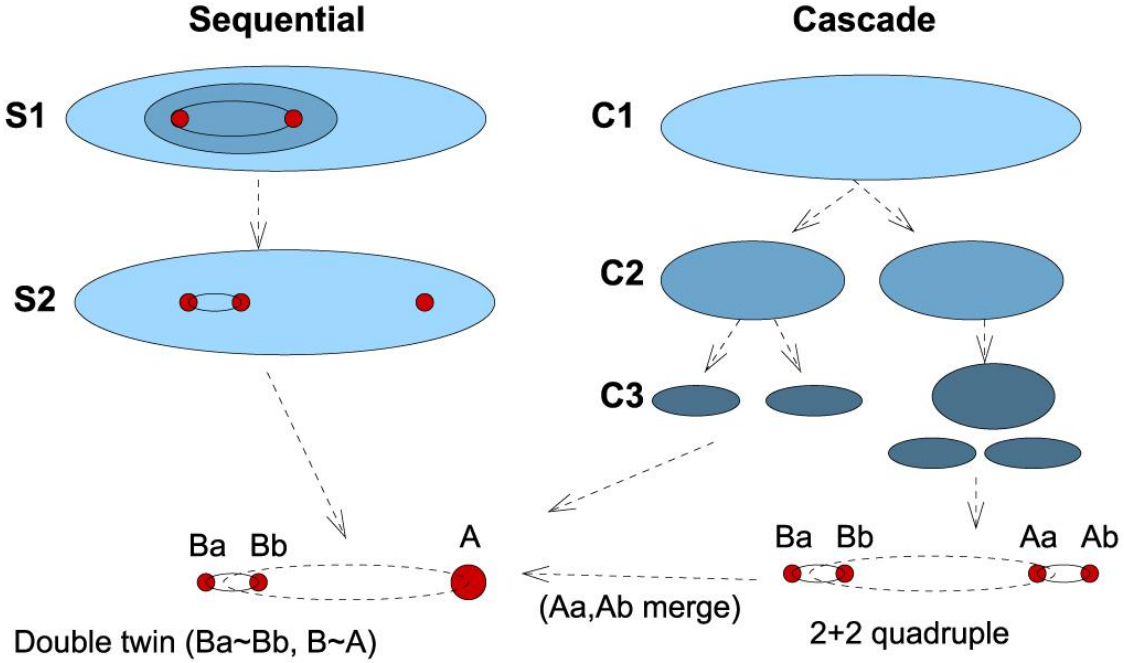

Table 1
Overview of Multiple Systems

WDS	HIP π (mas)	V (mag) Sp.type	Outer Name Inner Name	P (year)	a ($''$)	M_1 ($\mathcal{M}_\odot$)	M_2 ($\mathcal{M}_\odot$)	Φ ($^\circ$) P_2/P_1
00247–2653	…	15.4	LEI 1 A,BC	77.6	1.528	0.12	0.15s	1, 125
	129.5	M7V	LEI 1 B,C	17.25	0.460	0.077	0.070	4.50 ± 0.03
02022–2402	9497	7.88	HDS 272 A,B	80	0.414	1.44	1.22 s	27, 27
	16.09	F6V	TOK 41 Ba,Bb	14.4	0.102	0.64	0.58	5.6 ± 0.7
05239–0052	25240	6.11	WNC 2 A,BC	1200	3.716	2.73 s	2.62 s	17, 166
	18.75	F7V	A 847 B,C	47	0.337	1.07	1.55	~25
16057–3252	78842	8.34	SEE 264 A,B	131	0.807	0.96	1.50 s	14, 65
	24.70	K0V	WSI 84 Ba,Bb	10.5	0.128	0.75	0.75	12.6 ± 0.2

Note. Explanation of columns: (1) WDS code (Mason et al. 2001); (2) *Hipparcos* number and trigonometric parallax from various sources; (3) combined visual magnitude and spectral type from Simbad; (4) discoverer codes; (5) orbital period; (6) semimajor axis; (7) mass of the primary component; (8) mass of the secondary component (s means mass sum); (9) two values of mutual inclination Φ and the period ratio.

考察

- 今回の観測した4つの独立した階層系は、
  - 内側と外側の周期の比率
  - 偏心の小さい軌道
  - 内側と外側の伴星の質量

  等と共通点が多くある。
  このような階層は質量が増加する際に形成される、dynamicsによって生じたとは想像つきにくい。

- 1.5 $M_\odot$未満のMultiple Star Catalog(MSC)の隣接する階層レベルにおける質量比の比較
  Equal masses付近の濃度が濃く、Double-twin付近の濃度は薄くなっている。
  これより、3重星のすべてが同等の質量を有している可能性が大きくなる。

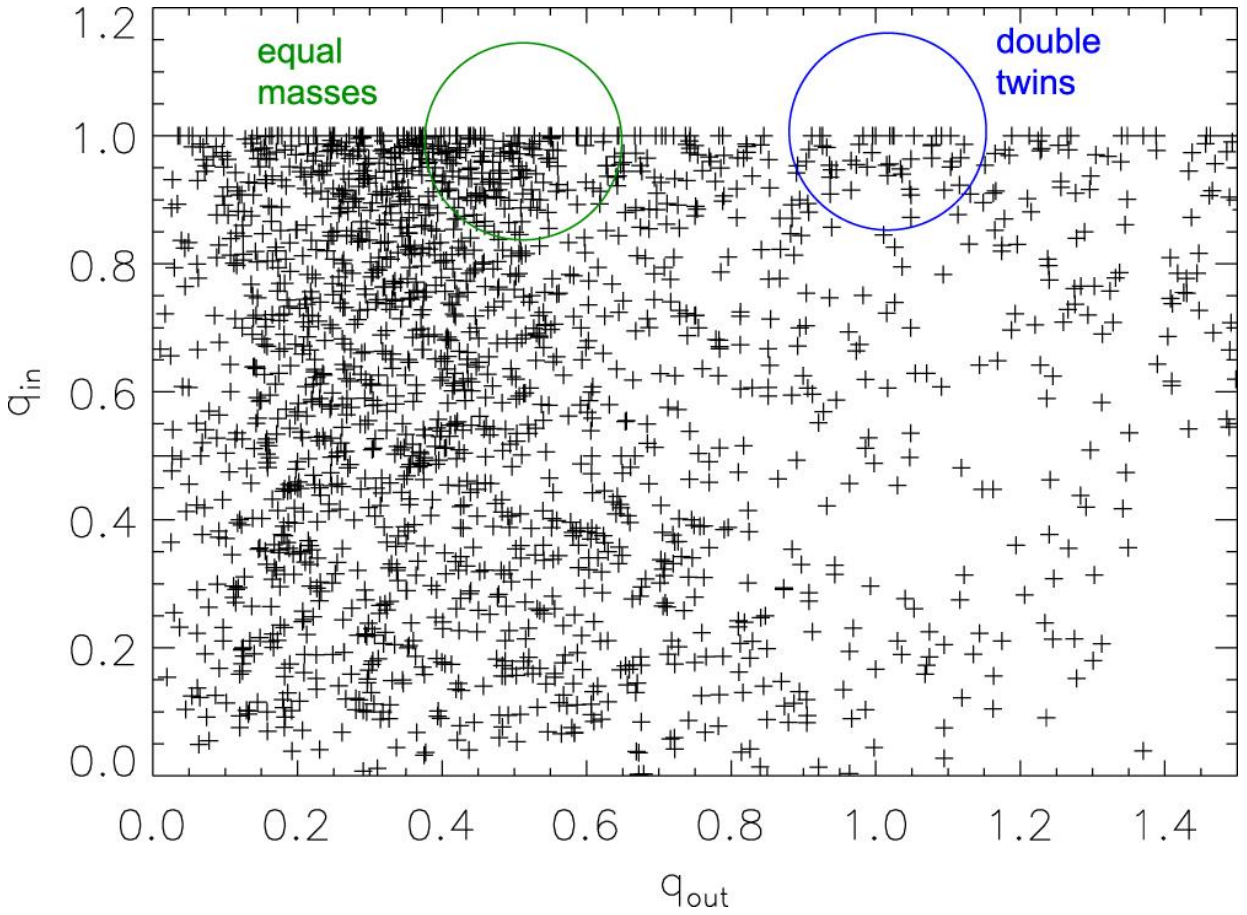

1.5 $M_\odot$未満のMultiple Star Catalog(MSC)で隣接する階層レベルにおける質量比の比較

#29 Unlocking CO Depletion in Protoplanetary Disks I. The Warm Molecular Layer

Kamber R. Schwarz, Edwin A. Bergin, L. Ilsedore Cleeves, Ke Zhang, Karin I. Oberg, Geoffrey A. Blake and Dana Anderson

ABSTRACT

CO is commonly used as a tracer of the total gas mass in both the interstellar medium and in protoplanetary disks.

Recently there has been much debate about the utility of CO as a mass tracer in disks.

Observations of CO in protoplanetary disks reveal a range of CO abundances, with measurements of low CO to dust mass ratios in numerous systems.

One possibility is that carbon is removed from CO via chemistry. However, the full range of physical conditions conducive to this chemical reprocessing is not well understood.

We perform a systematic survey of the time dependent chemistry in protoplanetary disks for 198 models with a range of physical conditions.

We varying dust grain size distribution, temperature, comic ray and X-ray ionization rate, disk mass, and initial water abundance, detailing what physical conditions are necessary to activate the various CO depletion mechanisms in the warm molecular layer.

We focus our analysis on the warm molecular layer in two regions: the outer disk (100 au) well outside the CO snowline and the inner disk (19 au) just inside the midplane CO snow line.

After 1 Myr, we find that the majority of models have a CO abundance relative to H2 less than $10-4$ in the outer disk, while an abundance less than $10-5$ requires the presence of cosmic rays.

Inside the CO snow line, significant depletion of CO only occurs in models with a high cosmic ray rate.

If cosmic rays are not present in young disks it is difficult to chemically remove carbon from CO.

Additionally, removing water prior to CO depletion impedes the chemical processing of CO.

Chemical processing alone cannot explain current observations of low CO abundances. Other mechanisms must also be involved.

#30 A Statistical Study of Massive Cluster-Forming Clumps

Tomomi Shimoikura, Kazuhito Dobashi, Fumitaka Nakamura, Tomoaki Matsumoto and Tomoya Hirota

ABSTRACT

We report results of the observations of 15 regions in several molecular lines for a statistical study of massive clusterforming clumps.

We identified 24 clumps based on the C18O (J = 1 − 0) data obtained by the NRO 45 m telescope, and found that 16 of them are associated with young clusters.

The clumps associated with clusters have a typical mass, radius, and molecular density of 1X103 Mo, 0.5 pc, 1X105 cm − 3, respectively.

We categorized the clumps and clusters into four types according to the spatial coincidence of gas and star density, and discussed their evolutions: Clumps without clusters (Type 1), clumps showing good correlations with clusters (Type 2), clumps showing poor correlations with clusters (Type 3), and clusters with no associated clumps (Type 4).

Analyses of the velocity structures and the chemical compositions imply that the clump + cluster systems should evolve from Type 1 to Type 4.

We found that some of the Type 2 clumps are infalling on the clump-scale to form clusters at the clump center, which should commonly occur in the beginning of cluster formation.

Interestingly, all of the identified Type 1 clumps are likely to be older than the Type 2 clumps in terms of chemical compositions, suggesting that they have been gravitationally stable for a long time possibly being supported by the strong magnetic field of >1 mG.

Type 1 clumps younger than the observed Type 2 clumps should be very rare to find because of their short lifetime.

#31 Sun-Sized Water Vapor Masers in Cepheus A

A.M. Sobolev, J.M. Moran, M.D. Gray, A. Alakoz, H. Imai, W.A. Baan,A.M. Tolmachev, V.A. Samodurov, and D.A.Ladeyshchikov

ABSTRACT

We present the first VLBI observations of a Galactic water maser (in Chepeus A) made with a very long baseline interferometric array involving the Radio Astron Earth-orbiting satellite station as one of its elements.

We detected two distinct components at −16.9 and 0.6 km s−1 with a fringe spacing of 66 microarcseconds.

In total power, the 0.6 km s−1 component appears to be a single Gaussian component of strength 580 Jy and width of 0.7 km s−1.

Single-telescope monitoring showed that its lifetime was only 8 months.

The absence of a Zeeman pattern implies the longitudinal magnetic field component is weaker than 120 mG.

The space-Earth cross power spectrum shows two unresolved components smaller than 15 microarcseconds, corresponding to a linear scale of 1.6 × 1011 cm, about the diameter of the Sun, for a distance of 700 pc, separated by 0.54 km s−1 in velocity and by 160 ± 35 microarcseconds in angle.

This is the smallest angular structure ever observed in a Galactic maser. The brightness temperatures are greater than 2 × 1014 K, and the line widths are 0.5 km s−1.

Most of the flux (about 87%) is contained in a halo of angular size of 400 ± 150 microarcseconds. This structure is associated with the compact HII region HW3diii.

We have probably picked up the most prominent peaks in the angular size range of our interferometer.

We discuss three dynamical models: (1) Keplerian motion around a central object, (2) two chance overlapping clouds, and (3) vortices caused by flow around an obstacle (i.e., von Karman vortex street) with Strouhal number of about 0.3.

#33 Triggering the formation of the supergiant HII region NGC 604 in M33

A. Kengo Tachihara, Pierre Gratier, Hidetoshi Sano, Kesetsu Tsuge, Rie E. Miura, Kazuyuki Muraoka and Yasuo Fukui

ABSTRACT

Formation mechanism of a supergiant HII region NGC 604 is discussed in terms of collision of HI clouds in M33.

An analysis of the archival HI data obtained with the Very Large Array (VLA) reveals complex velocity distributions around NGC 604.

The HI clouds are composed of two velocity components separated by ~ 20 km s−1 for an extent of ~ 700 pc, beyond the size of the the HII region.

Although the HI clouds are not easily separated in velocity with some mixed component represented by merged line profiles, the atomic gas mass amounts to 6 × 106 M⊙ and 9 × 106 M⊙ for each component.

These characteristics of HI gas and the distributions of dense molecular gas in the overlapping regions of the two velocity components suggest that the formation of giant molecular clouds and the following massive cluster formation have been induced by the collision of HI clouds with different velocities.

Referring to the existence of gas bridging feature connecting M33 with M31 reported by large-scale HI surveys, the disturbed atomic gas possibly represent the result of past tidal interaction between the two galaxies, which is analogous to the formation of the R136 cluster in the LMC.

#34 Helical Magnetic Fields in Molecular Clouds? A New Method to Determine the Line-of-Sight Magnetic Field Structure in Molecular Clouds

M. Tahani, R. Plume, J.C. Brown and J. Kainulainen

ABSTRACT

Magnetic fields pervade in the interstellar medium (ISM) and are believed to be important in the process of star formation, yet probing magnetic fields in star formation regions is challenging.

We propose a new method to use Faraday rotation measurements in small scale star forming regions to find the direction and magnitude of the component of magnetic field along the line-of-sight.

We test the proposed method in four relatively nearby regions of Orion A, Orion B, Perseus, and California. We use rotation measure data from the literature.

We adopt a simple approach based on relative measurements to estimate the rotation measure due to the molecular clouds over the Galactic contribution.

We then use a chemical evolution code along with extinction maps of each cloud to find the electron column density of the molecular cloud at the position of each rotation measure data point.

Combining the rotation measures produced by the molecular clouds and the electron column density, we calculate the line-of-sight magnetic field strength and direction.

In California and Orion A, we find clear evidence that the magnetic fields at one side of these filamentary structures are pointing towards us and are pointing away from us at the other side.

Even though the magnetic fields in Perseus might seem to suggest the same behavior, not enough data points are available to draw such conclusions.

In Orion B, as well, there are not enough data points available to detect such behavior.

This behavior is consistent with a helical magnetic field morphology. In the vicinity of available Zeeman measurements in OMC-1, OMC-B, and the dark cloud Barnard 1, we find magnetic field values of -23 ± 38 μG, -129 ± 28 μG, and 32 ± 101 μG, respectively, which are in agreement with the Zeeman Measurements.

#37 The Massive Star-Forming Regions Omnibus X-Ray Catalog, Second Installment

Leisa K. Townsley, Patrick S. Broos, Gordon P. Garmire, Gemma E. Anderson, Eric D. Feigelson,
Tim Naylor and Matthew S. Povich

ABSTRACT

We present the second installment of the Massive Star-forming Regions (MSFRs) Omnibus X-ray Catalog (MOXC2), a compilation of X-ray point sources detected in Chandra/ACIS observations of 16 Galactic MSFRs and surrounding fields.

MOXC2 includes 13 ACIS mosaics, three containing a pair of unrelated MSFRs at different distances, with a total catalog of 18,396 point sources.

The MSFRs sampled range over distances of 1.3 kpc to 6 kpc and populations varying from single massive protostars to the most massive Young Massive Cluster known in the Galaxy.

By carefully detecting and removing X-ray point sources down to the faintest statistically-significant limit, we facilitate the study of the remaining unresolved X-ray emission.

Through comparison with mid-infrared images that trace photon-dominated regions and ionization fronts, we see that the unresolved X-ray emission is due primarily to hot plasmas threading these MSFRs, the result of feedback from the winds and supernovae of massive stars.

The 16 MSFRs studied in MOXC2 more than double the MOXC1 sample, broadening the parameter space of ACIS MSFR explorations and expanding Chandra's substantial contribution to contemporary star formation science.

#38 Inward Migration of the TRAPPIST-1 Planets as Inferred From Their Water-Rich Compositions

Cayman T. Unterborn, Steven J. Desch, Natalie R. Hinkel and Alejandro Lorenzo Jr.

ABSTRACT

Multiple planet systems provide an ideal laboratory for probing exoplanet composition, formation history and potential habitability.

For the TRAPPIST-1 planets, the planetary radii are well established from transits (Gillon et al., 2016, Gillon et al., 2017), with reasonable mass estimates coming from transit timing variations (Gillon et al., 2017, Wang et al., 2017) and dynamical modeling (Quarles et al., 2017).

The low bulk densities of the TRAPPIST-1 planets demand significant volatile content. Here we show using mass-radius-composition models, that TRAPPIST-1f and g likely contain substantial (> 50 wt%) water/ice, with b and c being significantly drier (< 15 wt%).

We propose this gradient of water mass fractions implies planets f and g formed outside the primordial snow line whereas b and c formed inside.

We find that compared to planets in our solar system that also formed within the snow line, TRAPPIST-1b and c contain hundreds more oceans worth of water.

We demonstrate the extent and timescale of migration in the TRAPPIST-1 system depends on how rapidly the planets formed and the relative location of the primordial snow line.

This work provides a framework for understanding the differences between the protoplanetary disks of our solar system versus M dwarfs.

Our results provide key insights into the volatile budgets, timescales of planet formation, and migration history of likely the most common planetary host in the Galaxy.